THE AMERICAN SOCIETY OF MECHANICAL ENGINEERS
345 E. 47th St., New York, N.Y. 10017

97-GT-146

EXPERIMENTAL INVESTIGATION OF AN ATMOSPHERIC RECTANGULAR RICH QUENCH LEAN COMBUSTOR SECTOR FOR AEROENGINES

Peter Griebel

Michael Fischer, Christoph Hassa, Eggert Magens
Henning Nannen, Adolf Winandy
Institute for Propulsion Technology
German Aerospace Research Establishment
Cologne, Germany

Antigoni Chrysostomou, Ulrich Meier
Winfried Stricker
Institute for Physical Chemistry of Combustion
German Aerospace Research Establishment
Stuttgart, Germany

ABSTRACT

In this research work the potential of rich quench lean combustion for low emission aeroengines is investigated in a rectangular atmospheric sector, representing a segment of an annular combustor. For a constant design point (cruise) the mixing process and the NO_x formation are studied in detail by concentration, temperature and velocity measurements using intrusive and non-intrusive measuring techniques.

Measurements at the exit of the homogeneous primary zone show relatively high levels of non-thermal NO. The NO_x formation in the quench zone is very low due to the quick mixing of the secondary air achieved by an adequate penetration of the secondary air jets and a high turbulence level. The NO_x and CO emissions at the combustor exit are low and the pattern factor of the temperature distribution is sufficient.

INTRODUCTION

The rich quench lean combustion concept appears to be a hopeful candidate for low emission combustion in aeroengines. In the gas turbine, the concept was first applied to achieve low NO_x emissions using fuels with a high level of fuel-bound nitrogen, and was successfully demonstrated in Novick et al. (1982). Lew et al. (1982). In the USA the RQL concept has been chosen as one of the technologies in the HSCT program to achieve a low environmental pollution level (Shaw et al., 1993). In Germany basic studies of two stage combustion for industrial combustors were performed by Knapp et al. (1993). In a first step the Motoren und Turbinen Union (MTU) Munich investigated the emission reduction potential of a tubular combustor (Zarzalis and Ripplinger, 1992). In a second step a rectangular rich quench lean combustion sector for aeroengines was built and investigated in the Low Emission Combustion Technology project of the research program of the European Commission in co-operation with European partners. In this co-operation MTU designed and manufactured a sector and performed tests up to 15 bars. The German Aerospace Research Establishment (DLR) has built a second sector with identical geometry but with optical access to the mixing zone. In this sector the concentration, temperature and velocity field were measured with conventional and laser techniques. The results of these studies showed a remarkable NO_x reduction of 60 %, even at the non-ideal conditions of a recirculation of secondary air into the primary zone and a little underpenetration of the secondary air jets (Griebel et al., 1995, Koopman et al., 1996).

To study the emission reduction potential and the mixing and reaction in detail of rich quench lean combustion in aeroengines under ideal conditions, a second sector with a homogeneous primary zone and a redesigned mixing module was built and investigated. The studies were made for the fixed design point cruise, because this is the condition where the middle- and long-distance airplanes spent the most flight time and therefore generate the most NO_x emissions.

EXPERIMENTAL SET-UP AND TECHNIQUES

Set-up

Figure 1 shows a longitudinal cross-section of the experimental set-up seen from the side and the top. Air preheated up to 850 K is metered by critical nozzles in the inlet and divided in primary and secondary air. The kerosene fuel supply system is water-cooled and fuel preparation is achieved by a double row of twelve airblast nozzles. While the inner and outer airstream of one nozzle is co-rotating, the swirl direction of two neighbouring nozzles is opposite. The swirl of the primary air causes a recirculation zone, stabilizing the diffusion flame in the primary zone. The liner walls in the primary zone are convecively cooled with the secondary air, the liner walls in the secondary zone are film cooled. The liner wall temperatures were very uniform and in the primary zone they amount to 980 K. The secondary zone wall temperatures were about 900 K. The sidewalls of the combustor sector are convectively cooled with ambient air. To get optical

Presented at the International Gas Turbine & Aeroengine Congress & Exhibition
Orlando, Florida — June 2–June 5, 1997

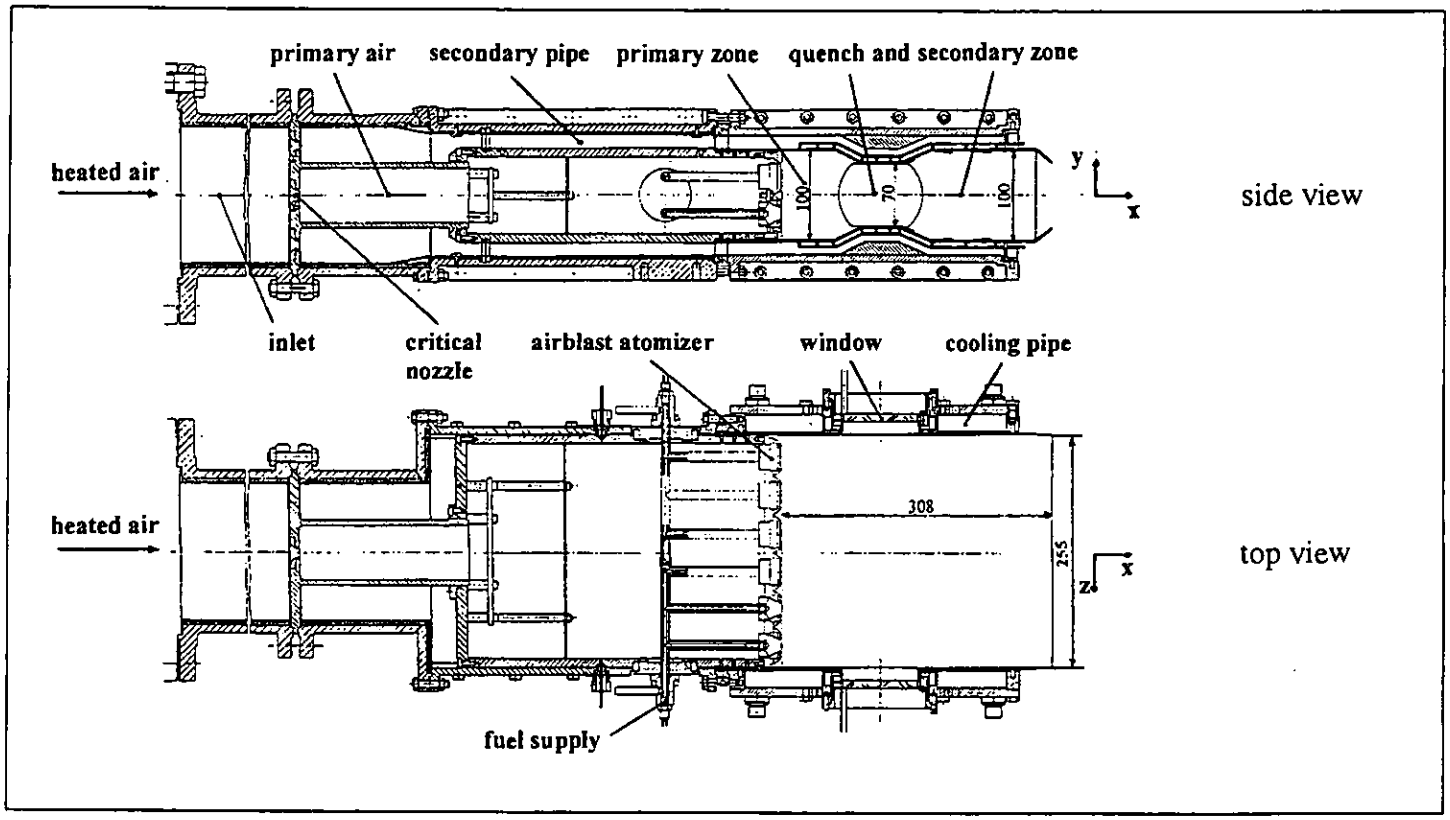

Fig. 1 Experimental set-up

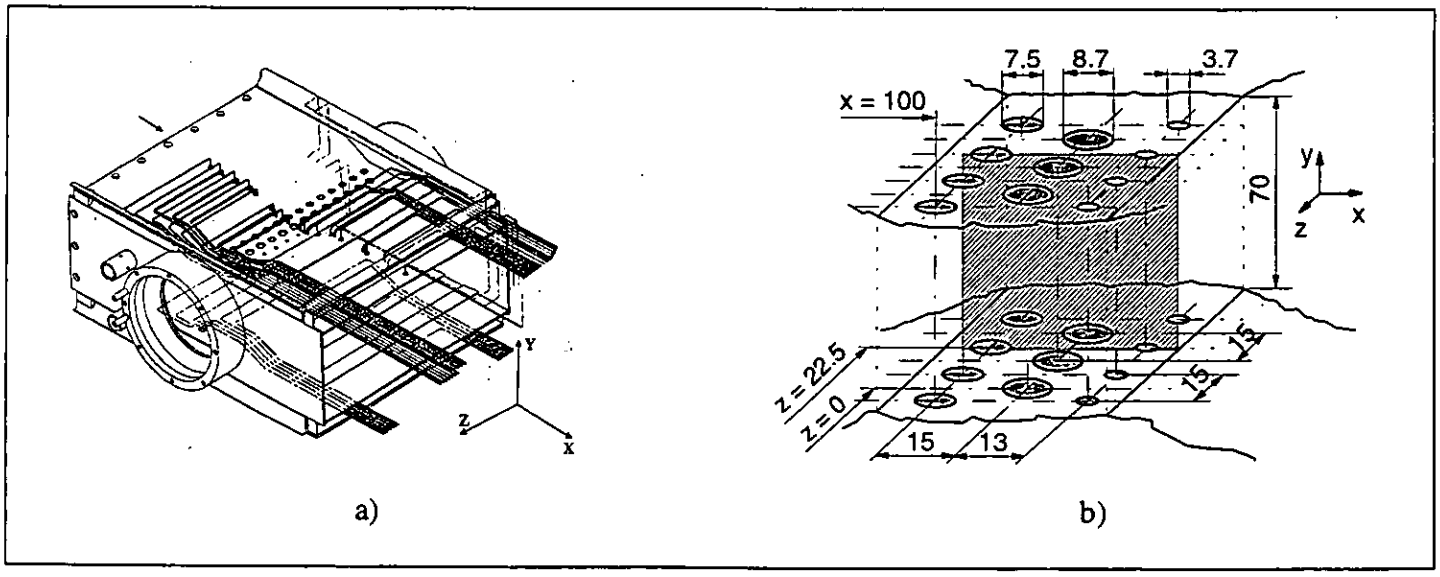

Fig. 2 Perspective view of the liner a) and the quench zone geometry b)

access for non-intrusive measuring techniques (CARS, LDV, LIF) two windows are mounted in the side walls of the quench zone. A detailed description of the set-up can be found in Nannen (1996). Figure 2 a) shows a perspective view of the rectangular liner. The secondary air is injected through three rows of holes, inline on top and bottom, as shown in figure 2 b). In the axial direction the rows have a staggered arrangement.

Measuring techniques

Conventional techniques. The local gas composition was measured using a suction probe and several analyzers for CO_2, CO, H_2, O_2, NO (NO_x), and UHC. For the correct NO_x measurements under fuel rich conditions, a special, heated converter with sufficient dilution of oxygen was used. The accuracy of the gas composition measurements was about 4 %.

The temperatures at the exit of the combustor were measured with a Al_2O_3 layered PtRh-Pt 30/6 thermocouple and corrected for radiation.

Laser Doppler Velocimetry. Velocities were measured with LDV in forward scattering using TSI (model 9107 and 9155) optics and Dantec electronics (model BSA). The airflow was seeded with titanium dioxide particles (< 1 µm), which are added at the inlet. The accuracy of the mean velocities was about 5 % (Hassa et al., 1996).

Coherent Anti-Stokes Raman Scattering. Temperatures were measured with a BOX CARS arrangement using single shot N_2 thermometry. The accuracy of the mean temperatures was about 3 % (Fischer et al., 1996).

Laser-Induced Fluorescence. Time-resolved spatial distributions of OH were recorded using planar laser-induced fluorescence (Kohse-Hoeinghaus, 1994). Fluorescence of hydroxyl radicals was detected following excitation in the A-X (1,0) band of OH around 284 nm with a pulsed tunable frequency-doubled dye laser.

RESULTS

The emissions behaviour was studied by a variation of the overall equivalence ratio, while keeping the air flow split constant. Therefore, an increasing primary zone equivalence ratio also causes a slight increase of the total equivalence ratio. The detailed measurements were all performed at the constant primary zone equivalence ratio of 1.64, which was a compromise between low NO_x and CO emissions (see figure 17) and avoided soot formation in the primary zone. The presented results were all measured in the representative sector between the z-positions z = 0 mm (axis of symmetry) and z = 45 mm, covering the periodicity of nozzles and mixing holes.

NO_x emissions and N-species

Figure 3 shows the mass averaged values of the emission index $EINO_x$ at the combustor exit and the N-species at the exit of the primary zone at several primary zone equivalence ratios (the values of the total equivalence ratios are added in brackets). For a better comparison, all values were calculated with the molar weight of NO_2.

The sum of the N-species, called Total Fixed Nitrogen, increases as the primary zone equivalence ratio decreases, because of the higher amount of thermal NO formed under conditions with higher temperatures and higher concentrations of oxygen. At an equivalence ratio of 1.38 the TFN consists only of NO. Under extremely fuel rich conditions the NO concentration is very low and the TFN consists mainly (max. 81 %) of the intermediate products HCN and NH_3. This is a consequence of the good primary zone homogeneity, that suppresses thermal NO formation, hence the non-thermal TFN parts dominate under those fuel rich conditions. The parameters influencing the non-thermal NO mechanisms are studied by numerical calculations, using several kinetic models and simulating the primary zone conditions of the experiment (stoichiometry, residence time, temperature, etc.). First results show a good agreement of the calculated HCN, NH_3 levels compared with the measured values, but an overestimation of NO concentrations (Frank et al., 1996).

A TFN minimum could not be found within the examined range of primary zone equivalence ratios. Perhaps it might exist on the fuel rich side of Φ_{Pz}= 1.77, but because of the entailing strong soot formation that is not of practical interest.

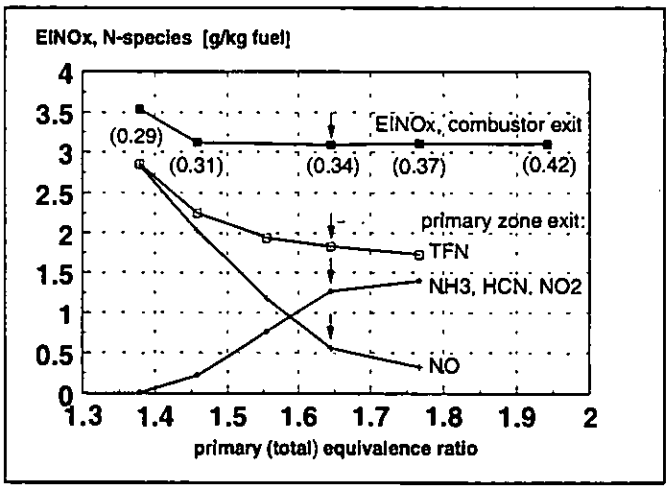

Fig. 3 $EINO_x$ at the combustor exit and N-species at the exit of the primary zone (mass averaged values)

The upper curve in figure 3 designating the integral of primary zone and secondary zone NO_x formation is not parallel to the TFN curve, but remains almost constant above Φ_{Pz} = 1.46. This is not too surprising, since the overall equivalence ratio and hence the secondary zone temperatures increase, while the primary zone TFN decreases, thus shifting a part of the overall NO_x production to the secondary zone.

A comparison of the measured emission index $EINO_x$ of 3.09 g/kg fuel at a primary zone equivalence ratio of 1.64 (marked in figure 3 with arrows) with the NO_x emission of a conventional combustor for aeroengines at take-off condition (ICAO 1993), shows a reduction by 63 %. For this comparison the NO_x emissions under the high pressure condition (pressure ratio 32) have been calculated with a correlation for the pressure dependency of NO_x ($\sim p^n$, n = 0.4). This exponent is in good agreement with Zarzalis, 1996, who had studied a similar combustor up to 15 bars.

Measurements at the primary zone exit

The double row of twelve airblast nozzles generates a good primary zone homogeneity preventing interactions of the recirculation zones with the secondary air. The distribution of the axial velocity at the exit of the primary zone in the representative sector is shown in figure 4.

Apart from a region between the positions y = +,- 15 mm and z < 15 mm, the axial velocity distribution is very homogeneous. The axial velocities reach the highest values near the upper and lower liner walls, forced by an acceleration of the flow due to the reduction of the combustor height. The lower axial velocities on the left side (z < 15 mm) are caused by a little deformation of the liner wall, which results in

higher jet angles of the first row of secondary air at these z-positions. Therefore the secondary air jets overpenetrate and form a small recirculation zone near the combustor axis (see figure 6).

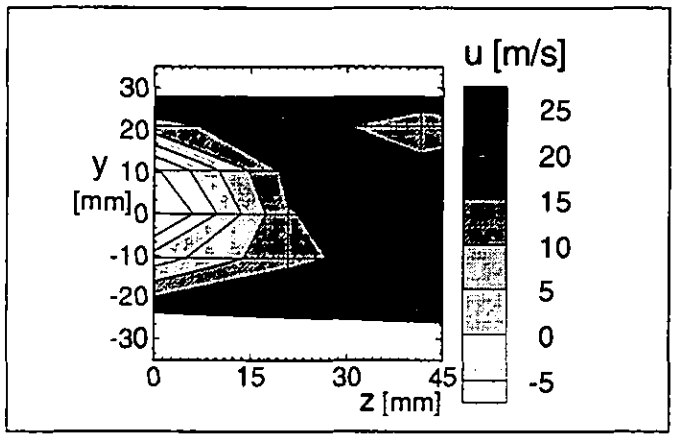

Fig. 4 Axial velocity at the exit of the primary zone

The extension of this recirculation zone reaches only a short distance upstream and the influence on the primary zone stoichiometry is quite small, which can be seen in the distribution of the equivalence ratio in figure 5. The recirculation leads to an increase of the equivalence ratio at the exit of the primary zone of only 7 %, compared with the global value. The slightly (about 1 %) higher equivalence ratios on the right side (30 mm < z < 45 mm) can be explained by a little non-uniformity of the fuel distribution of the twelve fuel nozzles.

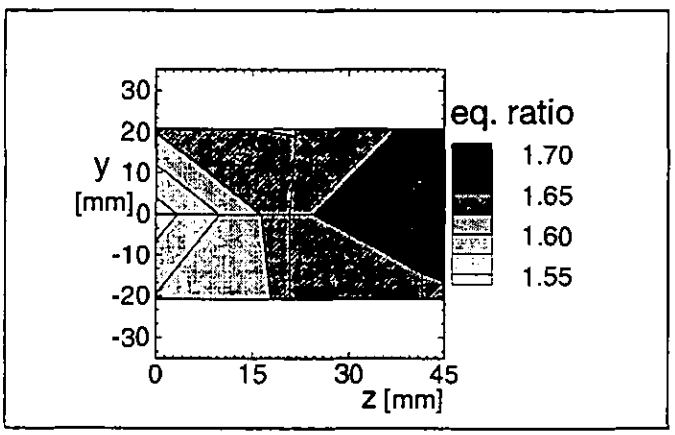

Fig. 5 Equivalence ratio at the exit of the primary zone

Measurements in the mixing zone

The small extension of the recirculation zone is shown in the axial velocity distribution in figure 6. This figure presents an axial section of the mixing zone, which cuts the middle of the holes of the first and the third secondary air jets (marked in the figure with filled arrows) at a position of z = 22.5 mm.

At the position of x = 96 mm the recirculation zone is already finished. The distribution of the axial velocity shows a good symmetry to the combustor axis, which indicates a uniform division of the secondary air into the upper and lower secondary pipe. Because of the symmetry, in the following figures only the upper part of the combustor (y > 0 mm) is presented.

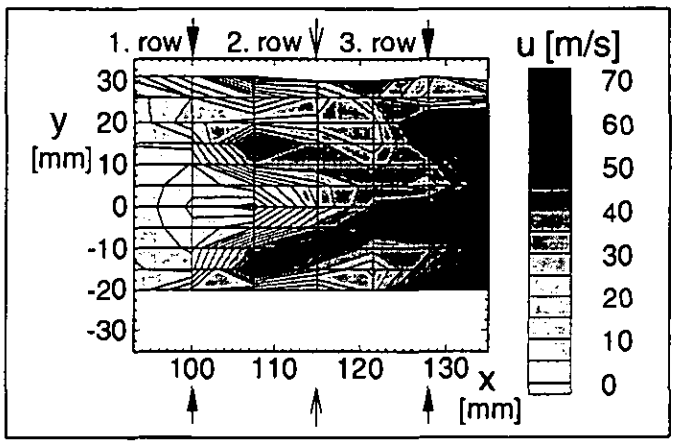

Fig. 6 Axial velocity in the cross-section z = 22.5 mm

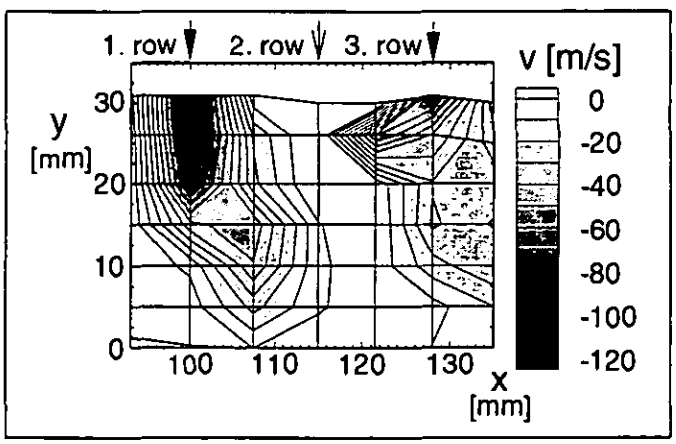

Fig. 7 Vertical velocity in the cross-section z = 22.5 mm

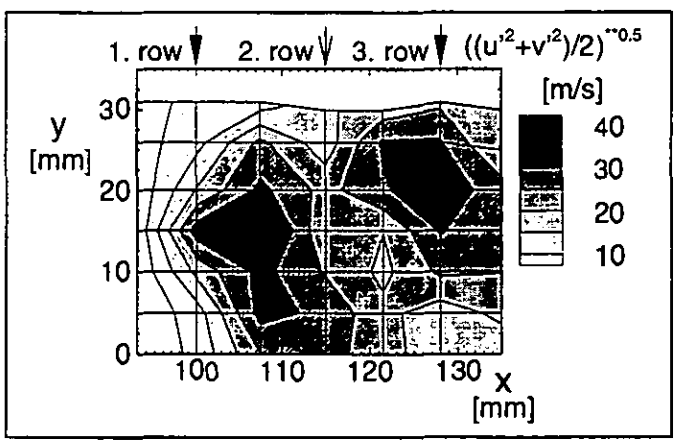

Fig. 8 RMS velocity in the cross-section z = 22.5 mm

The figures 7 and 8 show the vertical and the RMS velocities in the same x-y cross-section. The penetration of the first row of secondary air jets is sufficient to reach a good mixing in the near center region of

the combustor. The high turbulence level in the whole quench zone forces a fast mixing process with low NO formation in this zone. The highest RMS values of 40 m/s were found in the boundaries of the air jets, where the shear forces are very high.

CARS measurements in the quench zone were performed to gain information about the mean and peak temperatures dominating, besides the parameter residence time, the thermal NO formation. The figures 9 and 10 show the distribution of the mean temperature and the temperature PDF's at several positions.

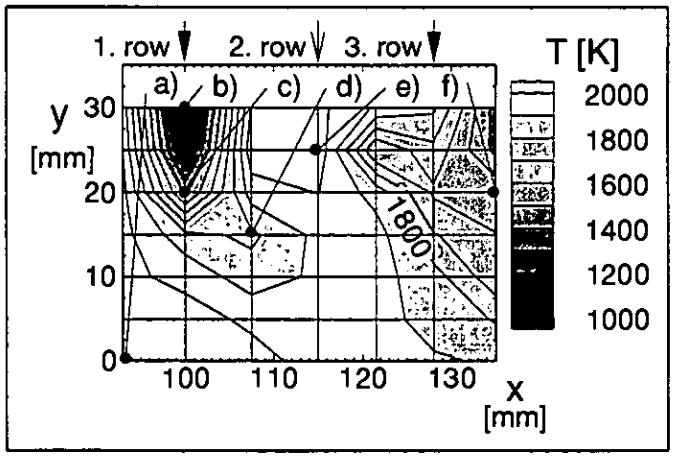

Fig. 9 Mean temperature in the cross-section z = 22.5 mm

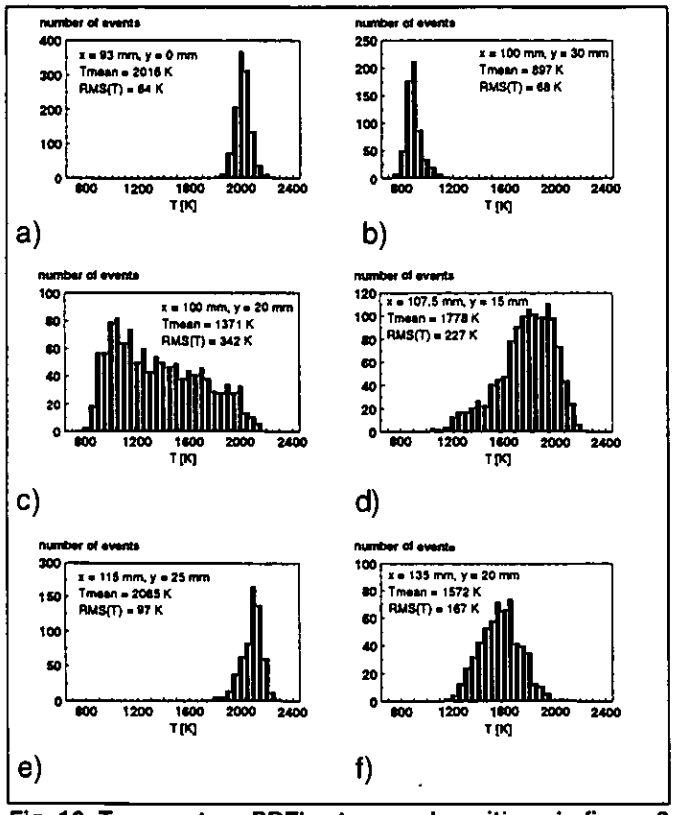

Fig. 10 Temperature PDF's at several positions in figure 9

Before the third row of the secondary air jets is added (x = 128 mm) the progression of the mixing process is nearly completed. Thus the temperature PDF's are symmetric and relatively narrow in this zone (see figure 10, f)) and the temperatures are below 1800 K almost over the whole combustor height. Therefore the thermal NO formation is low. Only in the near center region y < 12 mm the temperatures are still higher than 1800 K. The mean residence time in the quench zone, calculated with the bulk velocity and the quench zone length, is lower than 1 ms, which indicates a very fast mixing of the secondary air. The distribution of the mean temperature shows no regions of increasing mean temperatures even in the boundaries of the secondary air jets, where the heat release takes place (see figure 12). This stimulates the conclusion that at atmospheric pressure the turbulent mixing can be made intensive enough, so that at least on the average, the mixing is faster than the additional heat release. Under high pressure conditions the kinetics are much faster, therefore the mixing must be as quick as possible to prevent formation of hot spots, significantly contributing to secondary zone NO_x formation.

The highest temperatures (about 2000 K) and the narrowest temperature PDF's (figure 10, a)) were measured in a near center region (x < 115 mm and y < 5 mm), where unmixed primary zone exhaust gas still exists. This wedge, which is a typical pattern of an inline configuration, does not necessarily generate high NO emissions because of the low concentration of the oxygen radicals in this region. Other areas of high temperature (about 2080 K) and narrow PDF's (figure 10 e)) are the wakes of the air jets (for example: y > 25 mm, 110 mm < x < 115 mm), where unmixed primary exhaust gas can be found, recognizable of the low level of RMS temperatures in this region (see figure 11). Because of the blockage in the middle of the flame tube due to the secondary air jets, the primary zone exhaust gas escapes through the regions between the jet roots with an upward flow direction.

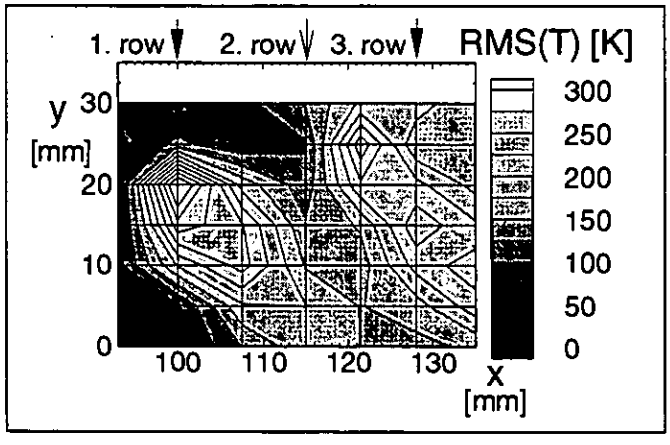

Fig. 11 RMS temperature in the cross-section z = 22.5 mm

A narrow and symmetric temperature PDF (figure 10, b)) with low mean temperature can be found in regions, where the cores of the secondary air jets are located (for example: x = 100 mm, y > 25 mm). The highest RMS temperatures (up to 300 K) were measured in the boundaries of the air jets, where the maximum RMS velocities occur too and where the temperature PDF's are wide and non-symmetric due to the high level of unmixedness. These regions consist of mixtures of primary zone exhaust gas and secondary air. If the primary zone exhaust gas dominates, the maximum in the PDF lies on the high

temperature side (figure 10, d)). If the secondary air dominates, the maximum lies on the low temperature side (figure 10, c)).

The simultaneous reaction and mixing in the quench zone is further elucidated by the distribution of the OH radicals of figure 12 in the circumferential cross-section through the first row of secondary air holes (x = 100 mm). The cores of the jets (positions marked with arrows), where no OH radicals occur can be seen clearly. The maximum OH concentration is located in a very thin layer of about 3 mm thickness at the jet boundaries, where the heat release takes place. A time series of about 120 pictures shows the stability of these structures with respect to area and time. Because of the deflection of the air jets in the axial direction and the orientation of the cross-section, defined by the laser light sheet, the lower boundaries of the jets can be seen too. That is the reason why these structures look like the character 'u'. The high level of OH radicals in the near center region of the combustor is due to the small recirculation zone, caused by the non-uniformity of the secondary air jets. Because of a recirculation of secondary air in this zone the equivalence ratio is lower and therefore the concentration of OH radicals is a little bit higher. The time series showed this region generally at a fixed position but with a strong temporal fluctuation of its shape, indicating a high turbulence level in this region.

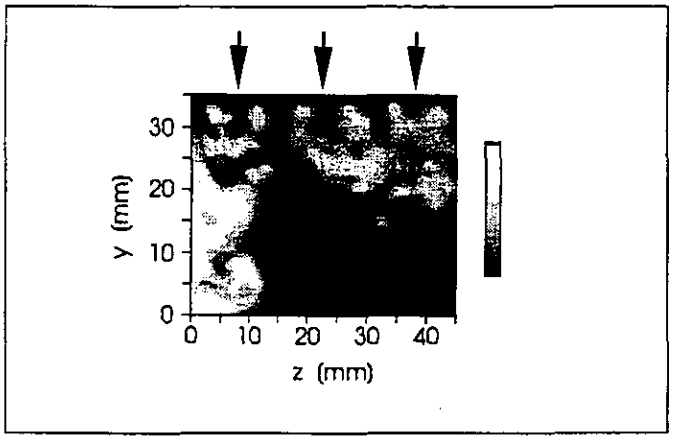

Fig. 12 Distribution of OH radicals in a cross-section through the first row of secondary air holes (x = 100 mm)

Finally in figure 13, the histograms of the equivalence ratio in five cross-sections at several x-positions are shown, such that the development of the spatial mixing process can be pursued.

At the exit of the primary zone the histogram of the equivalence ratio is very narrow, representing a homogeneous mixture.
After the first row of secondary air holes, the widest histogram of the equivalence ratio occurs, because the mixing process has just started. This cross-section consists of regions with nearly unmixed primary zone exhaust gas and those already partly mixed with secondary air. Most of the values lie between an equivalence ratio of 0.6 and 0.8, which is already on the fuel weak side.
In the cross-section after the second row of air jets no more regions of unmixed fuel rich primary zone exhaust gas can be found. The low equivalence ratios in this cross-section are due to the cores of secondary air jets, which were detected in the near wall regions.
The equivalence ratios in the fourth cross-section, at the exit of the quench zone (after the third row of secondary air holes), are all clearly on the fuel weak side of stoichiometry. Thus the thermal NO formation is very low. The histogram at this axial position is bimodal and because of the discrete successive addition of secondary air, it is bound to be bimodal somewhere, but it is narrower than the histogram of the previous cross-section, indicating that the mixing process is closer to the final state of a homogeneous mixture.

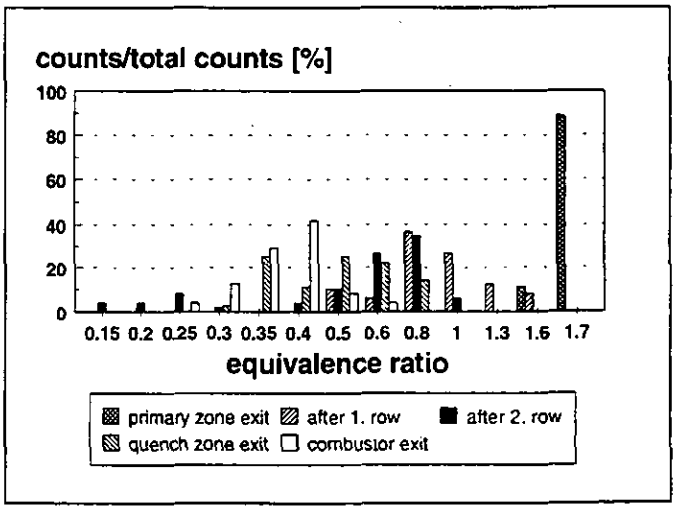

Fig. 13 Histograms of the equivalence ratio in cross-sections at five different axial positions

The histogram of the equivalence ratio at the combustor exit is narrow and nearly symmetric, with the highest counts at an equivalence ratio between 0.35 and 0.4. This is in good agreement with the total equivalence ratio of 0.36, which was the fixed global parameter of this experiment. The lower equivalence ratios in this cross-section have been found in the near wall regions and are due to partly mixed film cooling air.

The homogeneity in the circumferential direction is demonstrated in the figures 14 and 15, which present the distributions of the mean temperature and the equivalence ratio at the exit of the quench zone (x = 135 mm). The z-positions of the secondary air holes are marked with arrows (filled arrows symbolize the positions of the 1. and the 3. row, the unfilled ones represent the holes of the 2. row).

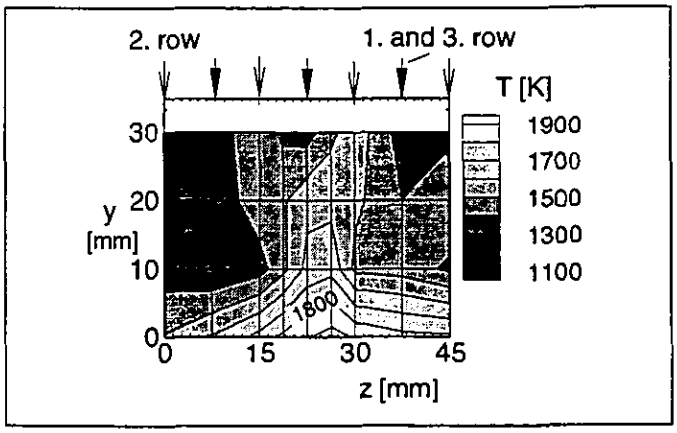

Fig. 14 Mean temperature at the exit of the quench zone

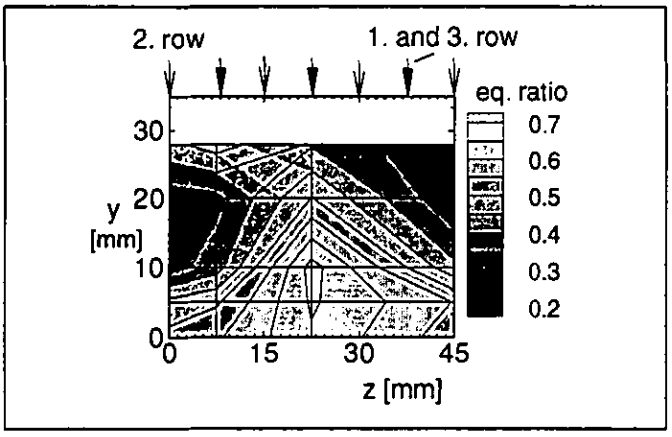

Fig. 15 Equivalence ratio at the exit of the quench zone

Apart from a small region at the axis of symmetry (y = 0 mm) of the combustor at the z-positions 19 mm < z < 38 mm, overall the temperature is lower than 1800 K and therefore the NO formation is very low.

The slightly higher temperatures at the position of z = 22.5 mm are due to a slightly different jet angle of the secondary air jet of the first row at this position, caused by a deformation of the liner wall. The orientation of this jet is shifted sidewards a little bit (+ z-direction) and therefore it fuses with the neighbouring jet, resulting in a lower turbulence level in this region because of the lack of shear layers. Therefore the progression of the mixing process in this area is slower, resulting in a slightly higher equivalence ratio and higher temperatures at the end of the quench zone. However the homogeneity at the exit of the quench zone is satisfactory.

Measurements at the combustor exit

Figure 16 shows the profiles of the emissions and the temperature at the axis of symmetry (y = 0 mm) at the combustor exit.

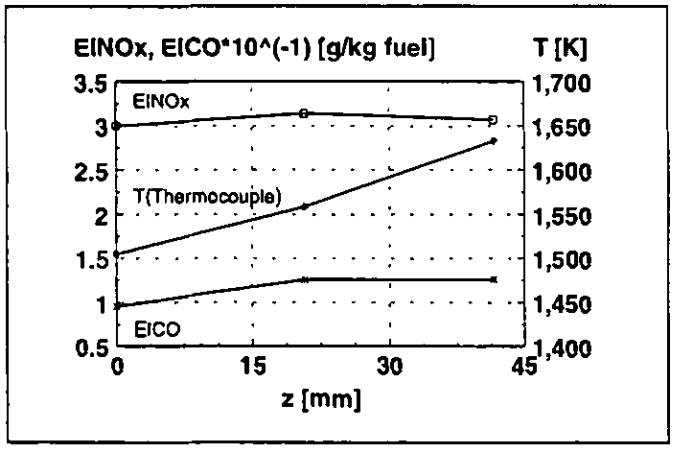

Fig. 16 NO_x, CO emission index and temperature at the exit of the combustor at y = 0 mm and several z-positions

The results of the measurements at several y-positions are very similar, therefore only the profiles at y = 0 mm are presented. At the exit of the combustor there is a great homogeneity and the emission index of NO_x is nearly constant. The CO emissions show a tendency of lower values on the left side (near the axis of symmetry z = 0 mm). The reason is again the non-uniform penetration of the secondary air jets, which causes a recirculation at this z-position at the exit of the primary zone. Therefore the temperatures in this recirculation zone are higher and the conditions for decomposition of CO are better than those of regions without a recirculation (z > 15 mm). Due to this recirculation the measured temperatures on the left side (z = 0 mm) are lower because of the advanced mixing in this area. In this recirculation zone the thermal NO formation increases due to an increase in residence time.

The distribution of the temperatures at the combustor exit is relatively homogeneous with a pattern factor of 0.19, which is an acceptable value for the inlet conditions of a turbine.

The behaviour of the mass averaged NO_x and CO emissions at a variation of the primary equivalence ratio is shown in figure 17. Again the values of the total equivalence ratios are added in brackets. The emission index of NO_x first decreases as the primary zone equivalence ratio increases due to a lower formation of thermal NO. For equivalence ratios higher than 1.46 the emission index of NO_x is nearly constant.

The emission index of CO shows a different behaviour. First the CO emissions decrease as the equivalence ratio increases. The reason of the higher CO values at lower primary zone equivalence ratios is the slower decomposition of CO at lower temperatures in the secondary zone due to lower total and therefore lower secondary zone equivalence ratios. At a primary zone equivalence ratio of about 1.75 the CO emissions increase as the equivalence ratio increases. This is caused by the high CO emissions of the primary zone under those extremely fuel rich conditions, which cannot be oxydized completely in the secondary zone because of a too short residence time.

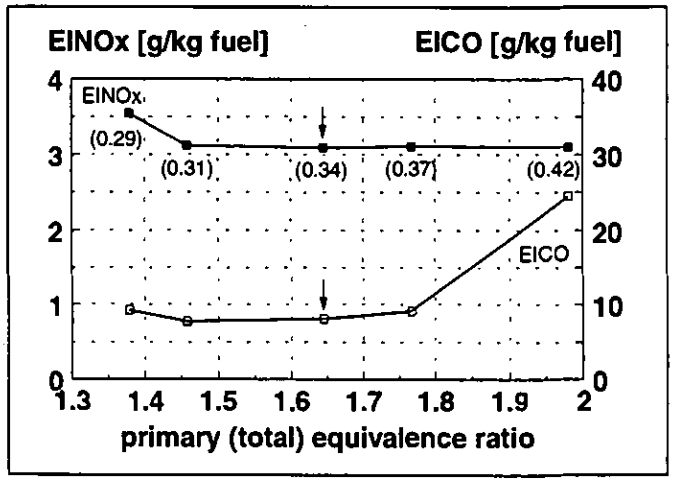

Fig. 17 Emission index of NO_x and CO at the exit of the combustor (mass averaged values)

Figure 17 shows a range of primary zone equivalence ratios, where both emissions, CO and NO_x are moderate and the curves are relatively flat. This shows the robustness of the rich quench lean concept providing an acceptable low emission band-width. At a primary zone equivalence ratio of 1.64 the measured emission index of NO_x was 3.09 g/kg fuel and 8.09 g/kg fuel for CO. It should be mentioned that the emission index of UHC was always zero in the measurements at the combustor exit.

CONCLUSION

The experimental fuel preparation system of a double row of twelve airblast nozzles generates a homogeneous mixture in the primary zone. Under extremely fuel rich conditions, the TFN at the exit of the primary zone consists mainly of HCN and NH_3, and NO is very low. In the range of the varied primary zone equivalence ratios, no TFN minimum at the exit of the primary zone can be found.

The results of the concentration, temperature and velocity measurements in the quench zone demonstrate a quick mixing process with low NO formation in the quench zone, resulting in a relatively homogeneous fuel weak mixture at the exit of the quench zone.

The temperature distribution at the combustor exit shows good homogeneity with a pattern factor of 0.19. The curves of the emission indices of NO_x and CO display a range of primary zone equivalence ratios, where both emissions, NO_x and CO are low. Therefore rich quench lean combustion has the ability for low emissions within a band-width of stoichiometry, which greatly facilitates the design and control of practical combustors.

The presented combustor has a remarkable NO_x reduction by 63 % compared with a modern conventional combustor.

Having demonstrated the atmospheric NO_x reduction potential, the future work will concentrate to preserve as much of that as possible, while choosing more practical components. The configuration planned, will have a single row of newly designed airblast nozzles, a shorter primary zone with an alternative cooling concept and further optimized mixing holes (Migueis, 1996).

LITERATURE

Novick, A.S., Troth, D.L., Yacobucci, H.G., 1982, "Design and Preliminary Results of a Fuel Flexible Industrial Gas Turbine Combustor", Transactions of the ASME, Vol. 104, pp.368-376.

Lew, H. G., DeCorso, S. M., Vermes, G., Carl, D., Havener, W. J., Schwab, J., Notardonato, J., 1982, "Low NO_x and Fuel Flexible Gas Turbine Combustors", Transactions of ASME, Vol.104, pp. 303-313.

Shaw, R. J., Gilkey, S., Hines, R., 1993, " Engine Technology Challenges for a 21st Century High Speed Civil Transport", ISABE 93-7064.

Knapp, K., Meisl, J. Leuckel, W., Wittig, S., 1993, " Reduzierung der NO_x-Emission in Gasturbinenbrennkammern durch zwei-stufige Verbrennungsführung", VDI-Berichte Nr. 1090, pp. 587-594.

Zarzalis, N., Ripplinger, T., 1992, "NO-Reduktion mittels der zweistufigen Verbrennung (Fett-Mager-Verbrennung) bei Gasturbinenbrennkammern", BWK, Bd. 44, Nr. 11.

Griebel, P., Behrendt, T., Hassa, C., Lückerath, R., Bergmann, V., Stricker, W., Zarzalis, N., 1995, "Untersuchung eines atmosphärischen Fett-Mager-Brennkammersektors für Flugtriebwerke", VDI-Berichte Nr. 1193, pp. 589-596.

Koopman, J., Griebel, P., Hassa, C., 1996, "Numerical and Experimental Investigation of a Rich Quench Lean Combustor Sector", ASME 96-GT-48.

Nannen, H., 1996, "Experimentelle Untersuchung eines atmosphärischen Fett-Mager-Brennkammersektors mit zweireihiger Anordnung der Luftstrom-Zerstäuberdüsen", Diplomarbeit, EBI Karlsruhe.

Hassa, C., Behrendt, T., Griebel, P., (1996), "LDA-Messungen in einem atmosphärischen Fett-Mager-Brennkammersektor für Flugtriebwerke", Lasermethoden in der Strömungsmeßtechnik, 5.Fachtagung der GALA, Shaker Verlag, Aachen, pp 35.1-35.7.

Fischer, M., Griebel, P., Magens, E., Winandy, 1996, "CARS temperature measurements in a rich quench lean combustion chamber for aeroengines", DLR report, IB-325-11-96.

Kohse-Hoeninghaus, K., 1994, "Laser techniques for the quantitative detection of reactive intermediates in combustion systems", Prog. Energy Combust. Sci. 20, pp 203-279.

Frank, P., Tan, T., Griebel, P., Nannen, H., Eickhoff, H., 1996, "Analysis of NO-Formation for Rich/Lean Staged Combustion", 3 rd Workshop on Modelling of Chemical Reaction Systems, Springer Series in Chemical Physics, (in print).

ICAO 1993, "Engine Exhaust Emissions Data Bank", DRA, Farnborough, First Edition

Zarzalis, N., 1996, "Rectangular RQL Combustor", Brite/Euram Low- Emission Combustor Technology research program, Task 1.2 final report.

Migueis, C. E., 1996, "Untersuchungen zur Optimierung der Mischzone einer fett-mager gestuften Ringbrennkammer", DLR-FB 96-33.